J. Mater. Eng. (1989) 11:141–147

Control of Zirconia Surface Phases in Annealed Alumina with Y^+/Zr^+ Implantation Ratios

J.K. Cochran, S.G. Pope, K.O. Legg, and H.F. Solnick-Legg

Abstract. In an effort to transformation toughen alumina surfaces, Y^+ was implanted in sapphire previously implanted with Zr^+ at a dose of 1.25×10^{17} ions/cm^2. The Y^+ implant doses ranged from 1 to 10×10^{15} ions/cm^2 and the double implants were labelled $Y^+/Zr^+/Al_2O_3$. Annealing in the air at 1400° C produced a uniform surface film of polycrystalline ZrO_2 doped with Y_2O_3 which had a grain size of 0.1 to 1.0 μm. From x-ray diffraction (XRD), the ZrO_2 phases transitioned from monoclinic to tetragonal to cubic as the Y_2O_3 content increased from 0 to 4 m/o based on zirconia content. Obtaining only cubic zirconia was surprising, because pure cubic ZrO_2 should result only above 9.2 m/o Y_2O_3. The ratios of Y to Zr measured by electron spectroscopy for chemical analysis (ESCA) depth profiling for the high dose Y^+ implant was equivalent to 10 m/o Y_2O_3 in ZrO_2 rather than the implanted ratio of 4 m/o. The higher than expected Y concentrations agreed with the XRD results and were probably produced by Zr removal by ion milling during the high Zr^+ dose implant. Surface fracture toughness, as measured by indentation, decreased as yttria content increased because elimination of monoclinic ZrO_2 from the precipitate phases prevented a surface compression layer created by the tetragonal to monoclinic ZrO_2 transition on cooling from annealing temperatures.

INTRODUCTION

The object of this study was to improve hardness, fracture toughness, and wear resistance of oxide surfaces by implanting species that would produce insoluble oxide precipitates on annealing in an oxygen containing atmosphere. To this end, the ZrO_2–Al_2O_3 system was used as a model because alumina is insoluble in zirconia and zirconia in alumina at temperatures below 1600° C [1]. In a previous study, Cochran et al. [2–4] implanted single crystal yttria-stabilized zirconia (YSZ) with 190 keV Al^+ ions at a dose of 4 E17/cm^2. On annealing in air from 1150 to 1575° C, precipitates of Al_2O_3 were produced in the YSZ surface, the microstructure of which could be manipulated by annealing schedule. The precipitate morphology appeared controlled by well separated nucleation–crystallization rate temperature ranges. If samples were annealed at 1400° C by rapid heating through the 1200° C nucleation temperature, few nuclei formed and large (≈1–5 μm) isolated platelike precipitates formed which increased the hardness and fracture toughness ≈25%. If samples were heat treated to increase nuclei density at an optimum nucleation time of 6 hr at 1200° C and then heat treated at 1400° C for crystal growth, fine interlocking ribbon-like precipitates formed that increased hardness ≈40% and fracture toughness ≈80%. The interlocking precipitate structure was termed a nucleation controlled microstructure (NCM).

When sapphire was implanted with Zr^+ at a dose of 1.25 E17/cm^2 and 150 keV, air annealling produced surface precipitates of monoclinic or tetragonal ZrO_2 which was identifiable by XRD [5]. As annealing temperature increased from 950 to 1400° C, the ZrO_2 precipitates increased in size from 50 to 500 nm and the room temperature precipitate phase transitioned from tetragonal ZrO_2 at the small grain sizes to monoclinic at large grain sizes. Where the precipitates were all monoclinic, hardness increases of 10%

J.K. Cochran and S.G. Pope are with the School of Materials Engineering, Georgia Institute of Technology, Atlanta, GA 30332-0245, USA. K.O. Legg and H.F. Solnick-Legg are with Ionic Atlanta, Inc., Atlanta, GA 30309, USA.

and fracture toughness increases of 20–30% were consistently demonstrated. Under these same conditions, Konoike [6] demonstrated that the flexure strength of 3 mm diameter sapphire rods could be increased 10% (from 750 to 825 MPa) by implanting with Zr^+ and annealing to produce ZrO_2 surface precipitates that were mainly monoclinic. The formation of compressive surface stresses caused by the expansion present during the tetragonal to monoclinic ZrO_2 phase transformation on cooling was proposed as the strengthening mechanism. In this study, Y^+ was implanted into sapphire that had previously been implanted with Zr^+. Implantation was followed by air annealing to precipitate Y_2O_3 doped ZrO_2. The Y_2O_3 surface concentrations implanted were designed to be in the same range (0–4 m/o Y_2O_3 based on ZrO_2 concentration) as have been found optimum for producing transformation toughening in alumina [7].

EXPERIMENTAL PROCEDURE

Ion Implantation

Single-crystal sapphire was implanted with Zr^+ at 150 KeV with a dose of 1.25 E17 ions/cm^2. After Zr^+ implantation, Y^+ was implanted also at 150 keV and at doses of 1.0, 1.5, 2.0, 2.5, 5.0, 7.5, or 10.0 E15/cm^2. A calculated depth profile for the 1.25 E17 Zr^+ implant is shown in Figure 1 and except for concentration levels, the depth profile for Y^+ implants is essentially the same since Zr^+ is the adjacent element and they have close to the same atomic mass. The $11\bar{2}0$ sapphire single crystals, 2.5 cm diameter × 0.1 cm thick, polished on both sides, from Crystal Systems, Inc., Salem, Massachusetts, were annealed at 1400° C for 24 hr and cooled at 100° C hr prior to implantation. For both zirconium and yttrium, the implants were carried out using a Freeman source. Pure metals were placed in intimate thermal contact with a tungsten filament and heated in a chlorine discharge. Beam currents of 50 μA were produced and electrostatically scanned over the 2.5 cm diameter sapphire disks. Implantation was by Ionic Atlanta, Atlanta, Georgia. Samples of each implant dose were annealed at 1400° C for 2 and 4 hr by heating to temperature in 3 hr and cooling to room temperature in 4 hr. After annealing, the ZrO_2 precipitate microstructure was observed in a scanning electron microscope (SEM).

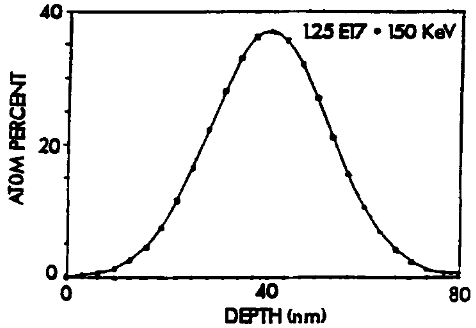

Fig. 1. Calculated depth profile for Al_2O_3 implanted with 1.25 E17 Zr^+/cm^2.

Depth Profiles

In addition to the depth profile calculated from (LSS) theory, Figure 1, depth profiles for Zr, Y, Al, O, and C were generated by ESCA [x-ray photoelectron spectroscopy (XPS)] analysis on unannealed samples implanted with 1.25 E17 Zr^+/cm^2 and no yttrium and one sample implanted with 1.25 E17 Zr^+/cm^2 and 10.0 E15 Y^+/cm^2. The depth profiles were generated by argon ion milling the surface and final etch pit depths were determined by interferometry.

X-ray Diffraction

A standard powder diffractometer was used to examine the crystallized ZrO_2 phases present for each anneal. Usable x-ray intensities were produced by the ~50 nm thick film from a powder diffractometer because a surface film of high x-ray absorption (ZrO_2) was on a substrate of low absorption (Al_2O_3). Cubic, tetragonal, and monoclinic ZrO_2 phases were found in the crystallized surface layer, the extent of each phase appearing to be related to yttria concentration. To provide optimum XRD traces, a scan rate of 0.125 deg 2θ/min at a time constant of 10 sec was used with a scale factor of 300 cps. This provided the maximum statistical advantage possible for our instrument.

Microhardness and Fracture Toughness

Indentation hardness and fracture toughness ratios were used to evaluate physical properties of the ion implanted and annealed samples. Each sample possessed an implanted and unimplanted region, and the ratio of indentation values from these regions was used as an indication of improvement or degradation due to the implant. All hardness and fracture toughness values were measured with a LECO-400 microhardness tester fitted with a Vickers diamond indenter. Vickers hardness and fracture toughness were calculated from 500 g load indentation diagonals and half-penny crack dimensions. Sample statistics recorded were the average and standard deviation for six measurements at each data point. Average errors for the ration values were the sum of the error from the implanted and unimplanted regions. Fracture toughness was calculated from [8]:

$$K_{Ic} = 0.016\,(E/H)^{1/2}\,(P/C_o^{3/2}) \qquad (1)$$

where *E* is Young's modulus, *H* is Vickers Hardness,

P is load, and C_o is the crack depth. The elastic modulus used for single crystal sapphire was 425 GPa [8].

RESULTS AND DISCUSSION

Precipitate Microstructure

Annealing the Zr^+/Al_2O_3 and the $Y^+/Zr^+/Al_2O_3$ implants at 1400° C for 2 and 4 hr produced a surface film of polycrystalline ZrO_2 with grain sizes ranging from ~0.1 to ~1.0 μm, Figure 2. The grain size distribution appeared to be bimodal with the majority grouped in the 0.1 to 0.4 μm size range. A smaller fraction of much larger 0.6 to 1.0 μm diameter thin grains, which may result from a substrate controlled preferred orientation, was also observed. In some cases, the surface ZrO_2 grains had a tendency to coalesce and expose the sapphire substrate. This coalescence appeared to be slightly greater for the 4 hr anneal compared to the 2 hr anneal but otherwise, microstructures for the two annealing times were similar.

Phase Analysis

Crystalline phase analysis of the 4 hr, 1400° C samples, Figure 3, by XRD indicated that the "Zr^+ only" sample contained only monoclinic zirconia with a (001) preferred orientation. The 2.5 E15 Y^+/cm^2 specimen exhibited only randomly oriented tetragonal ZrO_2 precipitates. The 5 E15 Y^+/cm^2 sample (2 m/o Y_2O_3) showed a combined tetragonal and cubic character after 4 hr at 1400° C. At a dose of 7.5 E15 Y^+/cm^2 (4 m/o Y_2O_3), the ZrO_2 precipitates were pure cubic with a strong (100) preferred orientation. Perhaps the large flat grains observed in the 10 E15 y^+/cm^2 samples, Figure 2(c), were the (100) oriented grains while the smaller grains were more randomly oriented.

When the phases present were compared with the Y_2O_3–ZrO_2 phase diagram [9], it appeared that the Y_2O_3/ZrO_2 ratio was approximately twice the ratio that had been intended. For example, the Y^+ and Zr^+ implants of 10 E15/cm^2 and 1.25 E17/cm^2, respectively, would provide a Y_2O_3 content of 4 m/o based on ZrO_2. The major phase for this composition should be monoclinic or tetragonal ZrO_2 (depending on grain size and cooling rate) with a minor cubic ZrO_2 component. As can be seen [observe the (400) type reflections where cubic and tetragonal ZrO_2 peaks are clearly separated] in Figure 3, the 10 E15 Y^+/cm^2 dose produced pure cubic ZrO_2 which should occur only at Y_2O_3 contents above ~9 m/o. This would indicate a Y_2O_3/ZrO_2 ratio in the implanted samples that was 2–2.5 times larger than measured from integration of ion beam currents.

In an attempt to produce implanted surfaces with Y_2O_3 contents in the range of 1.0 to 2.5 m/o, sap-

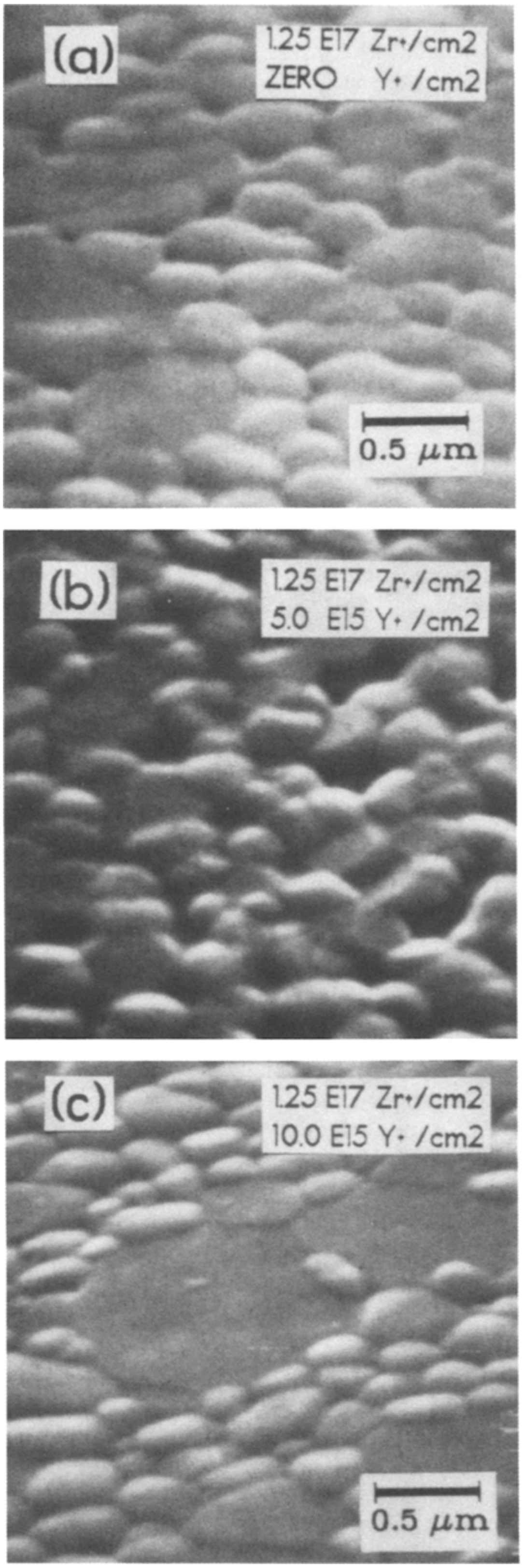

Fig. 2. Microstructure of Y^+/1.25 E17 Zr^+/Al_2O_3 annealed at 1400° C for 2 hr, (a) zero Y^+ (b) 5.0 E15 Y^+ (c) 10.0 E15 Y^+.

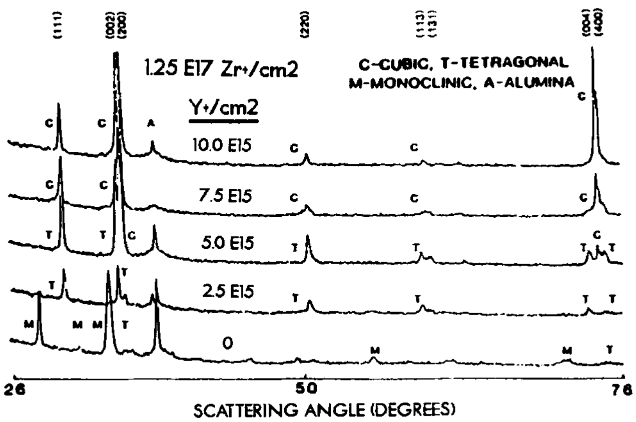

Fig. 3. XRD traces of sapphire implanted with 1.25 E17 Zr^+/cm^2 and Y^+ at doses from 0–10 $E15/cm^2$. Annealed at 1400° C for 4 hr.

phire samples were implanted with 1.25 E17 Zr^+/cm^2 and over-implanted with 1.0, 1.5, 2.0, and 2.5 Y^+/cm^2 both at 150 keV. After annealing at 1400° C for 4 hr, the surface precipitates produced the XRD patterns shown in Figure 4. The zirconia film for all these double implants was predominantly (100) and (001) oriented monoclinic ZrO_2. In addition, a minor tetragonal component with a (001) orientation was present and the tetragonal component did increase with Y^+ content. The tetragonal content for this 2.5 E15 Y^+/cm^2 dose did not appear to be as large as for the first 2.5 E15 Y^+/cm^2 sample shown in Figure 3. However, with the large degree of preferred orientation, accurate quantitative comparisons are not possible.

Depth Profiles

Depth profiles on as-implanted Zr^+/Al_2O_3 and $Y^+/Zr^+/Al_2O_3$ were measured using ESCA, Figures 5 and 6. Implant doses were 1.25 E17 Zr^+/cm^2 and 1.0 E16 Y^+/cm^2 both at 150 keV. Comparison of calculated and ESCA depth profiles based on maximum concentration at the peak, peak width at half height, and average implant are shown in Table 1. As can be seen, the experimental Zr contents are larger (50–58 a/o vs. 37 a/o) than calculated, as would be expected. The calculations do not consider the density reduction of the surface due to amorphization and expansion of the surface. At these high concentrations, the Zr profile has assumed a square shape as opposed to the classic Gaussian predicted by LSS theory. The square profile has been interpreted previously as resulting from stress induced diffusion which causes saturation of the surface. Diffusion away from the peak produces the square plateau profile.

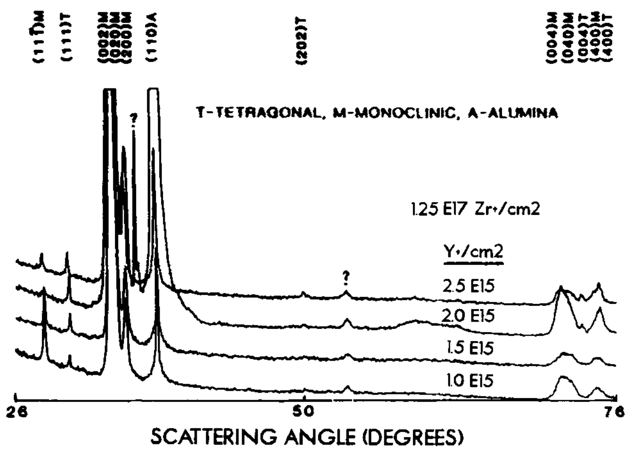

Fig. 4. XRD traces of sapphire implanted with 1.25 E17 Zr^+/cm^2 and Y^+ at doses from 1.0–2.5 $E15/cm^2$. Annealed at 1400° C for 4 hr.

Peak widths and depths from the two ESCA profiles, Figures 5 and 6, do not agree well, but both show the Zr concentration is high at the surface and extends to a depth of 400–600 Å. Thus, the surface crystallization of ZrO_2 was to be expected for annealing because the implants were not below the surface as would normally be expected but existed as a surface film in the as-implanted state.

The ratios of Y to Zr measured from the ESCA data for the double implant, Table 1, were sufficient to produce 10 m/o Y_2O_3 based on ZrO_2 content rather than the implanted ratio of 4 m/o Y_2O_3. The higher than expected Y^+ content may have been a result of Zr removal by ion milling during the high Zr^+ dose and the sequential Y^+ implant. The higher than expected Y concentration agrees with XRD results on annealed specimen where only cubic zirconia was detected after annealing as explained above. From a combination of ZrO_2 phases as determined by XRD plus ESCA data, the actual Y_2O_3 content was estimated and compared to implanted values based on integrated ion beam currrents, Table 2.

Fracture Toughness and Hardness

Fracture toughness and Vickers hardness ratios for the Zr^+/Al_2O_3 and $Y^+/Zr^+/Al_2O_3$ implants annealed at 1400° C for 2 and 4 hr are shown in Figures 7 and 8, respectively. As shown earlier [5], implanting Zr^+ in sapphire and annealing under these conditions results in a fracture toughness increase of 15 to 30%. As can be seen in Figure 7, the Zr^+ only implant did produce a 15 to 20% increase in toughness, but as the yttria content increased, fracture toughness showed a general decrease toward bulk values. All Vickers hardness ratios were within ±4% of unity, Figure 8. This is within measurement error and shows no effect of ion implantation on hardness. However, at 500 g loads, the Vickers indent diagonals were ~70 μm and penetration depth was ≈10 μm. Thus, the volume of the

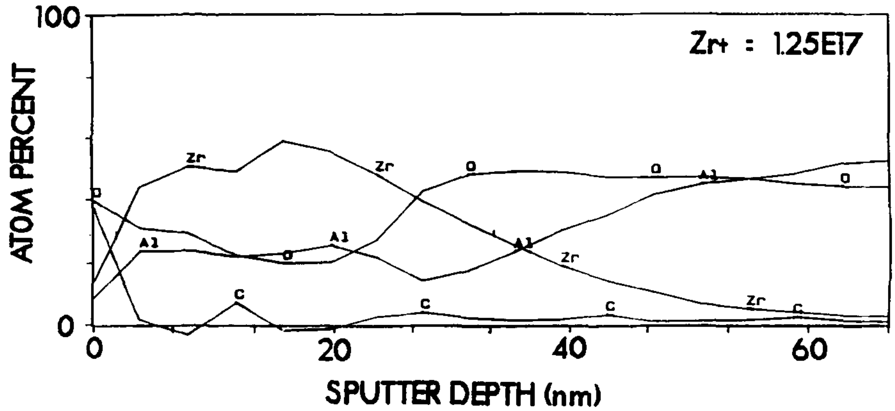

Fig. 5. ESCA depth profile of Zr^+/Al_2O_3 as-implanted at 1.25 E17 Zr^+/cm^2.

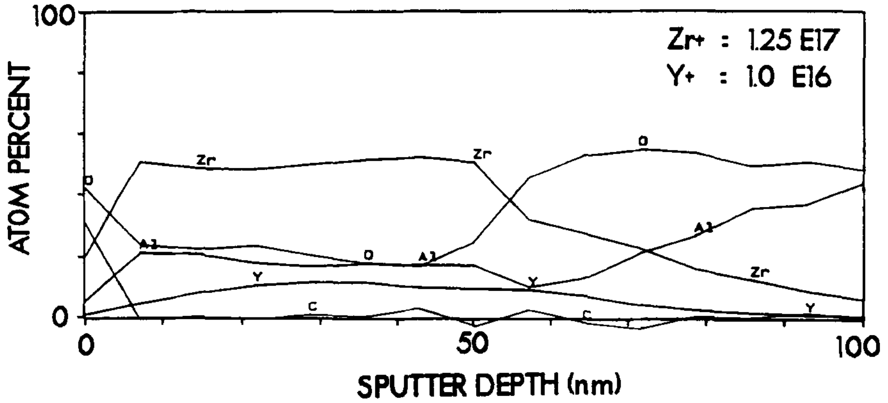

Fig. 6. ESCA depth profile of $Y^+/Zr^+/Al_2O_3$ as-implanted at 1.25 E17 Zr^+/cm^2 and 1.0×10^{16} Y^+/cm^2.

implanted layer with a thickness of ≈0.05 μm compared to the indent volume was insufficient to effect bulk hardness.

The yttria implant additions obviously reduced the fracture toughness compared to the Zr^+ implanted and annealed sapphire. Increases in K_{Ic} for Zr^+ only implants were thought to be caused by a compression layer resulting from the ≈7 v/o expansion of the tetragonal to monoclinic inversion on cooling plus an additional thermal expansion compression because the expansion coefficient of monoclinic ZrO_2 is less than that of sapphire. As yttria content increased and the monoclinic inversion was eliminated by stabilizing tetragonal and cubic ZrO_2, the compression layer was removed. In addition both tetragonal and cubic ZrO_2 have larger thermal expansion coefficients than sapphire and on cooling from annealing temperatures, a slight tensile surface layer would result from expansion mismatch.

It had been hoped that by producing a large tetragonal ZrO_2 component as was done by Y^+ doping,

Table 1. Zirconium and Yttrium Implant Concentrations and Distributions from Calculated and ESCA Results

Sample	Ion	Dose (ions/cm^2 × E16)	Peak Max. (a/o)	Peak Width (Å)	Avg. Depth (Å)
Calculated	Zr^+	12.5	37	290	420
Zr^+/Al_2O_3	Zr^+	12.5	58	310	180
$Y^+/Zr^+/Al_2O_3$	Zr^+	12.5	50	660	350
$Y^+/Zr^+/Al_2O_3$	Y^+	1.0	11	620	410

Table 2. ZrO_2 Phases and Y_2O_3 Concentrations for $Y^+/Zr^+/Al_2O_3$ Ion Implants at 1.25 E17 Zr^+/cm^2 and Annealed at 1400° C

Y^+ Dose (E15/cm^2)	ZrO_2[a] Phases (XRD)	Y_2O_3 Conc. Implanted (m/o)	Y_2O_3 Conc.[b] Probable (m/o)
0	M	0	0
1.0	M,T	0.4	1.0
1.5	M,T	0.6	1.5
2.0	T,M	0.8	2.0
2.5	T,M	1.0	2.5
5.0	T,C	2.0	5.0
7.5	C,T	3.0	7.5
10.0	C	4.0	10.5

[a] 1400° C, 4 hr.
[b] ESCA and XRD results.

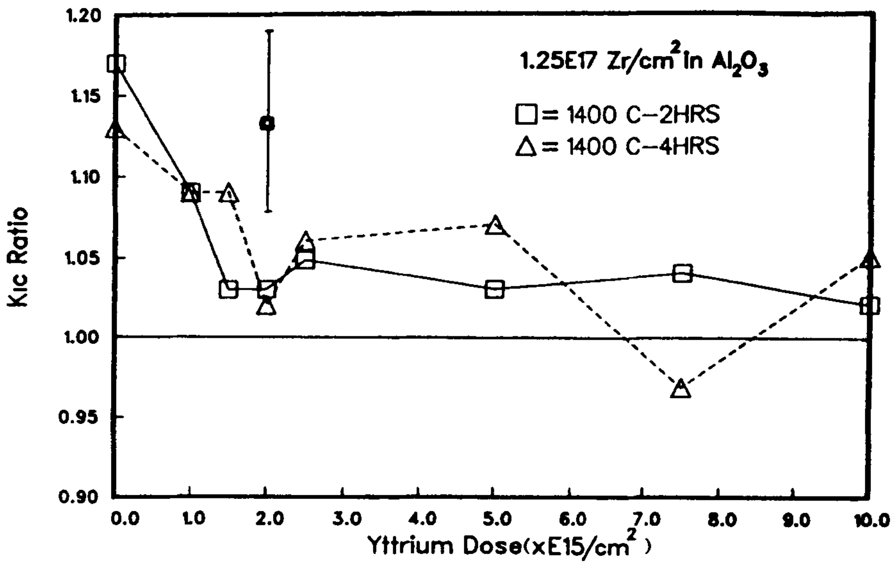

Fig. 7. Fracture toughness ratio vs. yttrium ion dose for sapphire implanted with 1.25 E17 Zr^+/cm^2 and annealed as indicated.

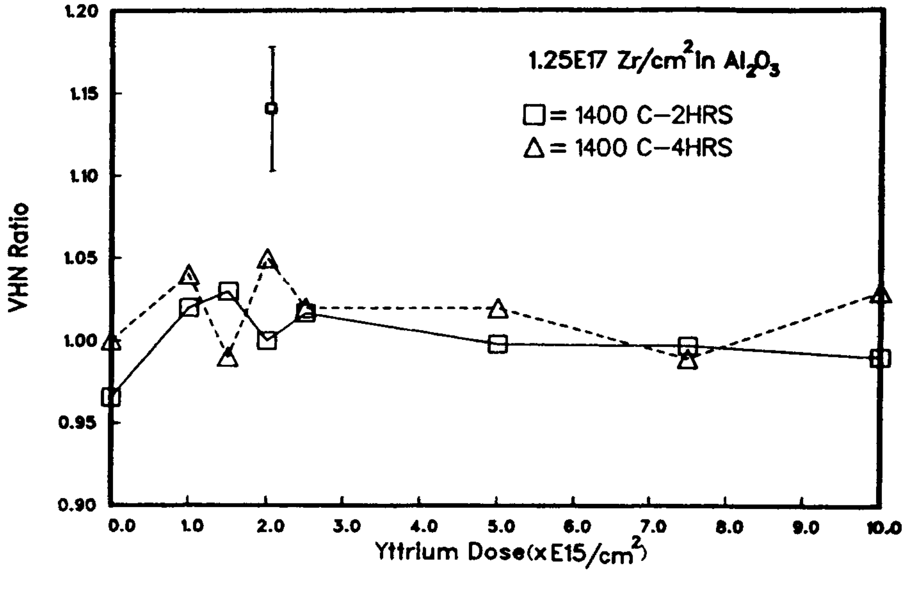

Fig. 8. Vickers hardness ratio vs. yttrium ion dose for sapphire implanted with 1.25 E17 Zr^+/cm^2 and annealed as indicated.

stress induced transformation would occur during cracking when fracture toughness was measured. This did not occur, probably because the ZrO_2 was on the surface and not dispersed in the alumina substrate. If ion implantation were at energies sufficient to place the Y^+ and Zr^+ at greater depths, producing tetragonal ZrO_2 by this means might provide stress induced transformation toughening.

CONCLUSIONS

It has been demonstrated that by ion implanting zirconium and yttrium in sapphire followed by air annealing, a polycrystalline ZrO_2 surface layer is produced where the ZrO_2 phases are monoclinic, tetragonal, or cubic depending on the Y^+ and Zr^+ ratio, as would be predicted by phase equilibria. It appears that significant ion milling occurs during the Zr^+ implantation which increases the Y^+/Zr^+ ratio by reducing Zr^+ content. Fracture toughness, as measured by indentation, decreased as yttria content increased because monoclinic ZrO_2 was eliminated from the precipitate phases. This prevented formation of a surface compression layer created by the tetragonal to monoclinic ZrO_2 inversion on cooling.

ACKNOWLEDGMENT

This work was supported by the Office of Energy Utilization Research, Energy Conversion and Utilization

Technologies Program, U.S. Department of Energy, under ORNL Subcontract 19BO7802C-X17 with Martin Marietta Energy Systems Incorporated.

REFERENCES

1. E.M. Levin and H.F. McMurdie, *Phase Diagrams for the Chemists Vol. III*, Diagrams 4377 and 4378, American Ceramic Society, Columbus, Ohio (1981).
2. J.K. Cochran, K.O. Legg, H.F. Solnick-Legg, and X.L. Mann, "Modification of Surface Properties of Yttria Stabilized Zirconia by Ion Implantation," *Nuclear Instruments and Methods in Physics Research* B 7/8, North Holland, Amsterdam, pp. 535–540 (1985).
3. J.K. Cochran, K.O. Legg, H.F. Solnick-Legg, and X.L. Mann, "Microstructural Control of Ion Implanted Ceramic Surfaces," *Proceedings 1985 ASEE Annual Conference*, L.P. Grayson and J.M. Biedenbach, eds., V2, pp. 602–608 (1985).
4. J.K. Cochran, S.G. Pope, K.O. Legg, and H.F. Solnick-Legg, "Ion Implantation Precipitate Microstructure and Mechanical Properties of Ceramic Surfaces," *J. of Mater. for Energy Systems, 8*, pp. 121–127, September (1986).
5. J.K. Cochran, K.O. Legg, H.F. Solnick-Legg, and S.G. Pope, "Toughening of Oxide Surfaces Through Ion Implantation," *Third Annual Report, D.O.E. ECUT Program*, ORNL Subcontract 19B07802C-X17, September (1986).
6. T. Konoike, "Strengthening of Single Crystal Alpha Alumina with Ion Implantation," M.S. Thesis, Materials Engineering, Georgia Institute of Technology, August (1986).
7. N. Claussen, "Microstructural Design of Zirconia-Toughened Ceramics (ZTC)," *Science and Technology of Zirconia II*, N. Claussen, M. Rhle, and A.H. Heuer, eds., American Ceramic Society, Columbus, Ohio (1984).
8. G.R. Anstis, P. Chantikul, B.R. Lawn, and D.B. Marshall, "A Critical Evaluation of Indentation Techniques for Measuring Fracture Toughness: I, Direct Crack Measurements," *J. Amer. Cer. Soc., 64*(9), pp. 533–543 (1981).
9. V.S. Stubican, R.C. Hink, and S.P. Ray, "Phase Equilibria and Ordering in the System ZrO_2–Y_2O_3," *J. Amer. Cer. Soc., 61*(1–2) pp. 17–21 (1978).